Impact of the Microstructure on Electrochemical Performances of Dilithium Benzoquinone Dioximate as a Positive Material for a Li-Ion Battery

Roberto Russo, Carine Davoisne, Adolfo Urrutia, Yann Danten, Carlo Gatti, Gwenaelle Toussaint, Philippe Stevens, Christine Frayret, Matthieu Becuwe

Impact of the microstructure on electrochemical performances of dilithium benzoquinone dioximate as positive material for Li-ion battery

Roberto Russo[a,b,c,f], Carine Davoisne* [a,c,f], Adolfo Urrutia[a,c,f], Yann Danten[d], Carlo Gatti[e], Gwenaelle Toussaint[b,c], Philippe Stevens,[b,c] Christine Frayret[a,c,f], Matthieu Becuwe*[a,c,f]

[a] *Laboratoire de Réactivité et Chimie des Solides (LRCS), UMR CNRS 7314, Université de Picardie Jules Verne, 15 rue Baudelocque, 80000 Amiens, France.*

[b]Yann *Department Electric Equipment Laboratory (LME), EDF R&D, Avenue des Renardières, 77818 Morêt-sur-Loing Cedex, France*

[c] *Réseau sur le Stockage Electrochimique de l'Energie (RS2E), FR CNRS 3459, Amiens, France.*

[d] *Institut des Sciences Moléculaires, UMR CNRS 5255, 351 Cours de la Libération, 33405 Talence, France*

[e] *CNR SCITEC, CNR Istituto di Scienze e Tecnologie Chimiche ''Giulio Natta'', Sede Via C. Golgi, 19, 20133 Milano, Italy*

[f] *Institut de Chimie de Picardie (ICP), FR CNRS 3085, 80039 Amiens, France*

Corresponding authors

Matthieu Becuwe, matthieu.becuwe@u-picardie.fr

Carine Davoisne, carine.davoisne@u-picardie.fr

Orcid

Roberto Russo : 0000-0003-4439-2520 ; **Carine davoisne:** 0000-0001-8660-9367 ; Yann Danten : 0000-0002-1994-2503; Carlo Gatti : 0000-0002-0047-1596; Gwenaelle Toussaint : 0000-0003-0964-143X ; Philippe Stevens : 0000-0003-2344-2699 ; Christine Frayret : 0000-0003-1732-1591 ; Matthieu Becuwe : 0000-0002-1949-3955

Keywords

Organic batteries, positive electrode, dioximate, self-polymerization, Transmission Electron Microscopy,

Abstract

Herein we would like to highlight the impact of the material microstructure on electrochemical performances of dilithium benzoquinone dioximate (Li_2-BQDO) and its oxidized and self-polymerized version (PNND), a promising electroactive material for energy storage application. Li_2-BQDO showed a reversible exchange of two lithium ions at high redox potential (3.0 V *vs.* Li^+/Li), acting as a lithiated organic positive electrode for lithium-ions batteries. After a preliminary computational study, electrochemical performance of the oxidized form of Li_2-BQDO, which polymerize inside the cell, were also investigated. Thanks to TEM analysis coupled with XRD experiment the role of microstructure and crystal structure in the energy storage process was highlighted.

Keywords: Benzoquinone dioxime, lithium-ion battery, organic electrode, Transmission Electron Microscopy

1. INTRODUCTION

In the last decade, the development of different chemistries for lithium-ion battery (LIB) technology have led to a considerable increase in the energy storage performance.[1,2] Nowadays, researchers are continuously improving the performance of various electrochemical aspects. However, the huge increase in ~~the~~ lithium ~~batteries~~ manufacturing, mainly driven by the automotive sector, is showing limits in terms of costs and impact on

natural resources. In fact, traditional lithium-ion batteries are based on inorganic-based materials[3], composed mainly of Ni, Co, V,… which are characterized by high extraction and processing costs, as well as poor and unfavorable geolocation. Finally, these materials are toxic and hardly recyclable, which leads to a relatively high environmental impact of production[4]. Therefore, in order not to nullify the advantages deriving from electric energy using storage materials with possible element shortage and price hike, it is essential to find alternative materials characterized by low costs and easy supply, as well as sustainable production with low environmental impact, but with adequate electrochemical properties to allow the development of technologies for mobility and electronics application.

In this context, organic materials made up of elements such as carbon, nitrogen and oxygen, extremely abundant on the earth's crust, easily available (some of them may be obtained directly from bio-sources) and low processing cost gained a huge success in the last few years.[5–7] Considering the enormous potential in energy storage applications, over the decades many organic materials have been developed, based on wide span of chemistry and redox-active groups. In particular, among the most studied it is possible to list the molecules that incorporate carbonyl groups, such as quinones, those based on nitrogen, such as imides and azo compounds, as well as derivatives of carboxylates[8–11].

Quinones are undoubtedly one of the most studied classes of organic compounds. The simplest structure among them is p-benzoquinone (p-BQ), composed of an aromatic ring with two oxygens substituents in para position. During the redox reaction, benzoquinone can be reduced by the insertion of two metal ions to form a hydroxyquinone salt. Following the reduction, the ring recovers its aromaticity, which leads to a significant lowering of the energy of the system. Furthermore, benzoquinones have shown an incredible versatility as they can be used for vast type of metal ions (Li^+, Na^+, K^+,…), structure can be easily modified through the facile addition of substituent on the aromatic ring to tune the (electro-)chemical properties

and can be obtained from bio-sources, making them advantageous from an economic and environmental point of view.[12] A final advantage of quinones is that they can serve as precursors for the creation of electroactive motifs. One example is TCNQ (7,7,8,8-tétracyano-p-quinodiméthane), which can be obtained from simple benzoquinone by condensation of Knoevenagel using malonitrile. This transformation leads to enhanced redox properties resulting from the electroactivity of the nitrile groups (3V vs Li).

Very recently, an electroactive molecule, easily synthesized by the action of hydroxyl amine on p-benzoquinone, was revealed as solid-state positive electrode for Li-ion batteries. [13] In this work, five lithiated dioxime (lithium dioximate) have been investigated and exhibited interesting electrochemical performance with redox around 2.5-3.2 V *vs.* Li^+/Li and capacity in the range of 210-360 mAh g^{-1}. In addition to the electrochemistry investigation, this work elucidated the redox mechanism of this class of compounds thanks to an *Ex-situ* infrared study and by using the diffraction technique to understand the role of the crystalline structure. It was proposed that the redox mechanism of the benzoquinone dioximate/poly-dinitrosobenzene (subsequently 1,4-Phenyleneazine-N,N-Dioxide) couple involves polymerization of the oxidized form while such aspect does not seems to affect the reversibility of the lithium ion de-/intercalation mechanism (Scheme 1).

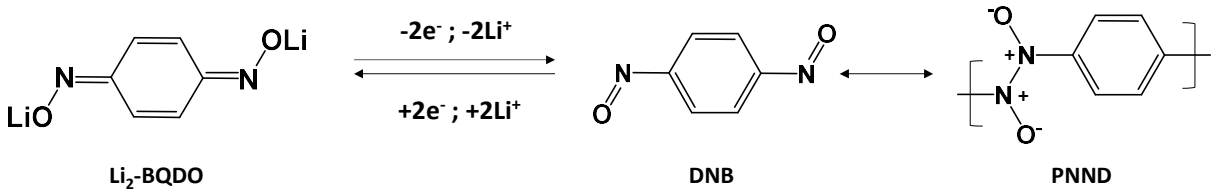

Li_2-BQDO DNB PNND

Scheme 1 - Electrochemical mechanism of lithium insertion/de-insertion involving di-lithium benzoquinone dioximate (Li_2-BQDO) (Left) and the poly *p*-dinitrosobenzene (PNND) (Right) /redox moieties.

Owing to the interesting discovery of this player in the field of redox active organic electrode material (OEM), it is of crucial interest to understand the nature of structure-activity

characterizing such backbone/redox center combination. This requires to proceed in several steps to disentangle distinct aspects that might influence electrochemical features. This is due in particular to the fact that such "C-nitroso compounds" (*i.e.* molecules having the nitroso group (R–N=O) attached to a carbon atom) present fascinating chemical features, which have drawn the attention of scientist's community. This system represents a molecular OFF-ON switch of the chemical bond between two nitrogen atoms, with an involvement of monomer-dimer equilibrium. Indeed, reactions of aromatic C-nitroso compounds can give rise to dimers in *Z* and *E* configurations thanks to photothermal "chemical switch", by which it is possible to break the chemical bond between two nitrogen atoms and bind them again. The possibility of occurrence of oligomerization and the above-mentioned polymerization of 1,4-dinitrosobenzene, with potential creation of shorter or longer chains, in which, depending on the conditions, the azodioxide group can appear either in its E- or in Z-form, leads to a very specific and complex situation in the context of electrochemistry, which is not the one of conventional OEMs. Prior to elucidating very precisely the structure-property relationships encompassing all these aspects, it is necessary to provide a first glimpse of how the monomers behave in the context of using such materials for their electrochemical properties. This will leave the opportunity, in a further study, to see the departure that can eventually occur from this simplest situation among distinct possible situations. In the present investigation, a quantum chemistry computation has thus been undertaken to first address the chemical reaction involving *p*-dinitrosobenzene (DNB) and di-lithium benzoquinone dioxime (Li_2-BQDO) monomers. From the experimental point of view, both Li_2BQD and its oxidized polymerized counterpart, (PNND), were synthesized and electrochemically characterized. The crystal structure of both compounds was then investigated using X-ray diffraction technique, while the microstructure of the crystals was observed with the TEM microscope, leaving the opportunity to understand its role in the lithium insertion/de-insertion process.

2. MATERIAL AND METHODS

2.1 Materials. p-Benzoquinone dioxime (95%) was supplied by Alfa-Aesar. $LiOH.H_2O$ (98%), $FeCl_3 \cdot 6H_2O$ (97%) and HCl solution (36%) were purchased by Sigma-Aldrich. All solvents were purchased dry from Sigma-Aldrich.

2.2 Synthesis. All the starting materials, intermediates and final products of Li_2-BQDO and PNND were characterized by ^1H NMR and FTIR spectroscopy. The infrared spectra, recorded in transmission mode and NMR spectra are reported in the supporting info (Fig. S3-S6).

2.3 Analytical and Electrochemical characterizations. The infrared spectra (FTIR) were acquired in transmission mode in the range 400-4000 cm^{-1}, using a Nicolet Avatar 370DTGS spectrometer, with a resolution of 2 cm^{-1}. The spectra were recorded by analyzing IR pellets, which were prepared by mixing active material and potassium bromide KBr (Sigma Aldrich, spectroscopic grade) in a ratio of 1:100. The powder mixture was pressed with a 13 mm evacuable die set (Specac Ltd, UK), resulting in an IR pellet. ^1H and ^{13}C NMR spectra were recorder with 400 MHz Avance III HD spectrometer (Bruker Co., US), equipped with a cryosonde. All the spectra reported in the present work have a chemical shift (δ) in ppm relative to tetramethylsilane (TMS). All the solvents employed for NMR analysis were purchased from Sigma Aldrich (99.9% D atom). The powder measured used to measure X-ray powder diffraction was cycled electrochemically, recovered, washed, ground and placed into a zero-background sample holder. The X-ray powder diffraction patterns were collected on a Bruker D8 Advance diffractometer with a Cu $K\alpha_1$ and $K\alpha_2$ radiation and equipped with a Lynkeye detector operating at 40 kV and 40 mA in between 2θ = 10-60° with a 2θ step size of 0.019° in reflection geometry. Although a zero-background sample holder was used, the inhomogeneous background is a result of residual amorphous material from the composite electrode and was included in the Pseudo-Voigt profile function refinement.

Thermogravimetric analyses (TGA) were performed on a Netzsch thermal analyzer STA 449C Jupiter equipped with a differential analysis microbalance coupled with a mass spectrometer QMS 403 Aeolos (heating rate: 5 °C min^{-1} under argon flow). The lithium content in the salts was determined by atomic absorption spectroscopy (AAS). The measurement was carried out using the AAnalyst 300 spectrometer (Perkin-Elmer, USA), equipped with a lithium hollow cathode lamp (wavelength: 670.8 nm), using a mixture of air/acetylene as oxidant/fuel with 5.8/1 ratio. The morphological and chemical analyses were performed using a Quanta 200 scanning electron microscope (FEI, Thermo-Fisher, USA) equipped with a X-ray energy dispersive spectroscope (X-Max 80, Oxford Instruments Co., UK). A few milligrams of active material powder were deposited on double-sided carbon tape, adhered to the SEM sample holder. The microstructural and chemical investigations at different charging state were performed using a transmission electron microscope TECNAI F20 STWIN working at 200kV and equipped with an X-ray energy dispersive spectroscope (X-Flash 6 TI 60, Bruker) and a GIF Tridiem (GATAN) for electron energy loss spectroscopy (EELS). The cycled sample were transferred from the glovebox to the TEM without air exposure according the procedure detailed by Dupont *et al.*[14] The cristallographic information were obtained through selected area electron diffraction. The EELS was performed with 1–1.2 eV energy resolution, a dispersion of 0.2 eV/channel, a conversion and a collection angle of 5.8 and 21.7 mrad, respectively. The energy loss near edge structure (ELNES) acquisitions were performed in STEM mode in defocus to limit the electron beam interaction. All the energy losses presented an error of ±0.2 eV. The electrochemical activity of the active materials was investigated in half-cell vs lithium metal through galvanostatic tests, performed with Swagelok-type cell. The cells were assembled under an inert atmosphere, inside a glovebox filled with argon, with controlled content of H_2O and O_2 (less than 0.1 ppm). The electrodes were prepared mixing 7-11 mg of active material (70% wt% of the composite

electrode) with 30% wt% of conductive carbon type Ketjenblack EC-600JD (AkzoNobel, Netherlands). The two components were mixed through 30 minutes of ball-milling. The negative electrode was made with a lithium metal disc, punched from a commercial lithium metal sheet (99.9% based on trace metals, Sigma-Aldrich). The positive electrode and the lithium disk were separated with a glass fiber separator (Whatman®), soaked with 150 ml of 1 M LiPF6 solution in ethylene carbonate:dimethyl carbonate 1:1 wt% (electrolyte LP30 , certified battery purity, Merck), as electrolyte. All cells were galvanostatic tested using a biological VMP-3 (Biologic SAS, France).

3. RESULTS AND DISCUSSION

3.1 Preliminary theoretical investigations. Density Functional Theory (DFT) calculations have become very common in the field of OEMs for batteries to complement the characterization of experimental works or even to take part in elucidating the mechanisms. As a first insight focused on the monomers DNB and Li_2-BQDO (Scheme 1), a molecular DFT modelling complemented by a thorough electronic structure analysis was undertaken to provide an initial glimpse of the redox phenomena in this class of materials. At the molecular state, for a redox system containing two active centers as it is the case here and by considering two successive steps each involving one electron/one Li^+, the redox mechanism can be envisioned similarly to the suggestion of Rathore *et al.*[15], or alternatively, instead of two successive one-electron/one Li^+ steps, one can suspect that the reaction may involve either only a single reduction or a direct double reduction. In such context, the description of the electrochemical features can be reached by focusing on three species: the “initial” (oxidized) form fully devoid of neighboring Li^+, an “intermediate” (singly reduced) form and a “final” (doubly reduced) form exhibiting an environment of two Li^+, each of them being located in the vicinity of each of the redox centers. Within the electrochemical process, the molecular

species presented in scheme 1 may evolve from the oxidized state , *i.e.* DNB, containing two N=O redox centres, towards the fully reduced state, *i.e.* Li_2-BQDO, characterized by an uptake of two electrons and involving a complex structure with two Li^+, which are supposed to be located in the neighborhood of each of the oxygen atoms, if one considers a direct double reduction. The present computational approach considers the two options of reaching either an uptake of one electron (single reduction) or directly two electrons (double reduction) starting from the oxidized specie. Within these electrochemical processes, the two following molecular species presented in scheme 1 are involved: the oxidized state , *i.e.* DNB, containing two N=O redox centres, and the fully reduced state, *i.e.* Li_2-BQDO, characterized by an uptake of two electrons and involving a complex structure with two Li^+, which are supposed to be located in the neighborhood of each of the oxygen atoms, if one considers a direct double reduction.

In view of gaining a preliminary insight on the way Lithium may locate in the vicinity of the DNB to form a complex entity upon reduction (*i.e.* Li_2-BQDO) for a reaction simply involving monomers, the Electrostatic Surface Potential (ESP) maps have proven to constitute a precious tool. [16]. The minima are more specifically meaningful since they constitute areas that are characterized by an accumulation of electron, where Li^+ ions may lie. The ESP maps of the three species that are involved during the electrochemical process of reduction of DNB are gathered in Figure 1, which concomitantly presents the representation of the three relaxed systems along with the corresponding bond lengths. Especially, focusing on the ESP map of DNB, it is straightforward to identify two minima, both located nearby each redox center, at ~ -22.3 and ~ -26.7 kcal/mol, within the red area exhibiting an electron-rich area. Among these two minima, the highest absolute value is situated in the vicinity of oxygen atom while the other one is nearer to the nitrogen atom. Each minimum is situated at a roughly equivalent distance from either the oxygen or nitrogen atom although the distance from the minimum at

~ -22.3 kcal/mol is slightly farther from nitrogen compared to the distance between oxygen and the minimum at ~ -26.7 kcal/mol. Upon either one/two electron(s) uptake, the molecular entity evolves towards a complex involving one/two Li^+ interacting with the oxygen(s) atom(s) of the mono-/di-anion through electrostatic interaction, which is clearly reflected in the ESP landscape. This latter is indeed modified accordingly, ending up with the doubly reduced state Li_2-BQDO which is characterized by a large red area covering the anion. The "intermediate" state corresponding more precisely to the singly reduced complex exhibits on the unreduced redox center a single minimum at ~ -55.6 kcal/mol nearby the oxygen atom. It is straightforward to identify that the Li^+ positioning effectively takes place within this area forming an almost linear arrangement with the C-N chemical bond (Figure 1) and thus constituting a kind of double chelation with Li^+ interacting preferentially with Oxygen but also with Nitrogen located however a bit farther (and presumably being less charged than Oxygen). The DFT modelling confirms and quantifies the geometrical structures of the two Li^+ complexes hypothesized through the ESP maps of DNB (Figure 1). Beyond these aspects, further characterization on the mechanism was gained thanks to an accurate electronic structure analysis based on the approaches developed in prior works[REFERENCES] (see ESI for full details).

REFERENCES : Lambert, F.; Danten, Y.; Gatti, C. ; Bocquet, B. ; Franco, A.A. ; Frayret, C. Carbonyl-Based Redox-Active Compounds as Organic Electrodes for Batteries: Escape from Middle−High Redox Potentials and Further Improvement? *Journal of Physical Chemistry A*, 2023, *127*, 5104-5119.

Lambert, F.; Danten, Y.; Gatti, C.; Frayret, C. A Tool for Deciphering the Redox Potential Ranking of Organic Compounds: A Case Study of Biomass-Extracted Quinones for Sustainable Energy. *Physical Chemistry Chemical Physics,* 2020, *22*, 20212–20226.

The main learnings accessible through this methodology correspond to the following observations: i) the simple representation of the redox process proposed in Scheme 1 (for the part indicating the sole consideration of monomer entities) is in fact slightly oversimplified in case of redox reactions considered between Li_2-BQDO and DNB; a slightly revised model for this mechanism has been proposed in which the Nitrogen atom is involved for the charge transfer effects and chelation of Li^+, which is consistent with the location of Li^+ in between the two ESP minima nearby the NO group ; ii) the redox potential estimated for the double reduction is consistent with a classification of this moiety within the positive OEMs; iii) the analysis of various indices gives an explanation of this classification, by highlighting the stabilization induced thanks to the redox center moiety upon lithiation of DNB, which counterbalance and even overcome the lack of aromaticity within the ring; iv) the DNB is characterized by a lower HOMO-LUMO gap than *p*-benzoquinone.

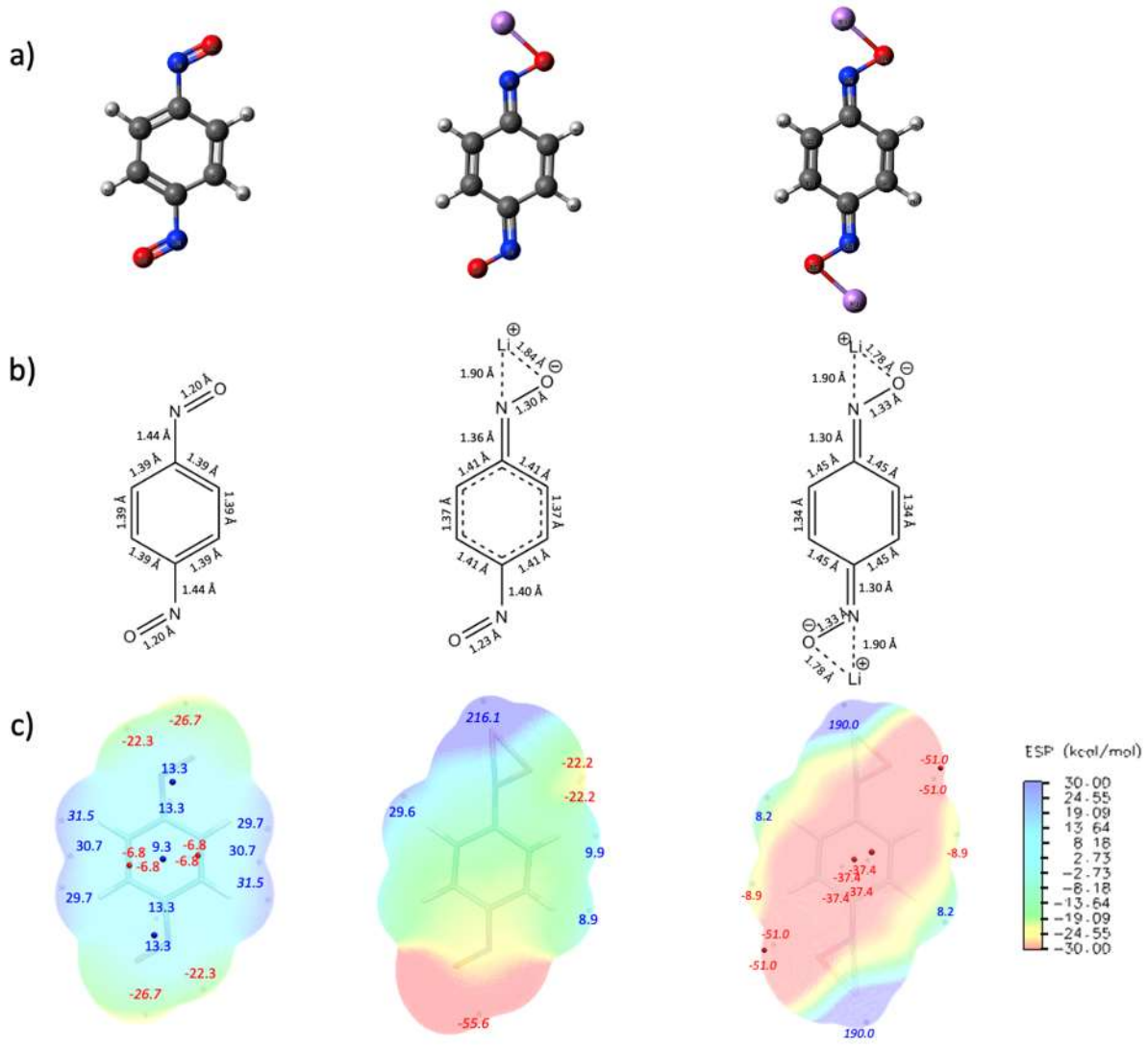

Figure 1: Evolution of systems from DNB towards Li_2-BQDO upon Lithium reduction according to the electrochemical mechanism proposed in Scheme 1: "Initial" or oxidized state (left), "intermediate" or singly reduced state (middle, Li-BQDO) and "final" or doubly reduced state (right, Li_2BQDO). a) DFT-computed structures b) interatomic distances indicated on the optimized geometry and c) Electrostatic surface potential (ESP) maps. Color code: blue (red) to visualize electron depletion (electron accumulation) within the range of 30.0 (deep blue)/-30.0 (deep red) kcal/mol. Surface local minima and maxima are represented along with corresponding values. See also Figure S1-2 for additional calculations.

3.2 Synthesis of dilithium benzoquinone dioximate and its oxidized version. In parallel with this modelling investigation, dilitihum 1,4-benzoquinone dioximate (**Li_2-BQDO**) were synthesized *via* salt formation reaction. To do so, benzoquinone dioxime (**BQD**) was reacted with $LiOH.H_2O$ in methanol (Scheme 2), using the same procedure reported for the lithiation of dihydroxybenzene.

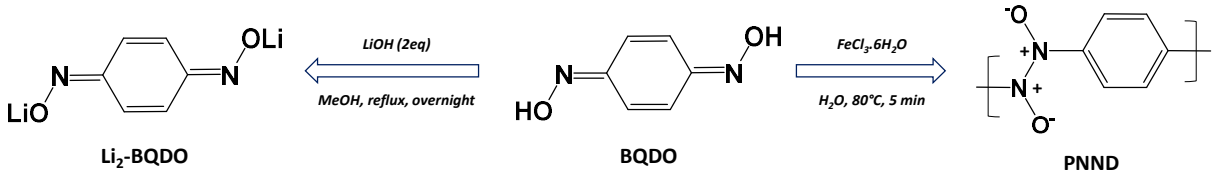

Scheme 2 - Synthetic routes of Dilithium benzoquinone dioximate (Li_2-BQDO) and Polydinitrosobenzene (PNND) from Benzoquinone dioxime.

The synthesis of Li_2-BQDO was confirmed by FTIR and NMR analysis. NMR spectrum (Supporting info, Figure S3-4) after the lithiation showed the disappearance of O-H peaks located at 12.10 ppm (s, 2H), observed in the pristine material (Supporting info, Figure S3). Furthermore, the aromatic hydrogen located were shifted at upfield (7.00-6.58 ppm) due to the presence of lithium ions, compared to the peaks in the BQD spectrum, located in the 7.85-6.44 ppm range (Figure S4). FTIR spectra (Figure S5a) corroborate the complete lithiation of benzoquinone dioxime. Disappearance of the O-H stretching band (around 3500 cm^{-1}) after lithiation and the shifting of C-N stretching peak from 991 cm^{-1} in BQD to 970 cm^{-1} in Li_2-BQDO, due to the presence of lithium ions is observed. Lithium content was measured using atomic absorption spectroscopy (AAS) analysis, giving a complete chemical formula of $Li_{2.03\pm0.05}$-BQDO. Finally, a thermogravimetric analysis (TGA, Figure S5b) was employed to determine the thermal stability and the degree of solvation. The analysis showed a no weight loss to 200 °C, where then its loss of the total mass. Moreover, we can deduce that the synthesized molecule is not in a solvated state and so can be used for electrochemical tests. The oxidized counterpart of dioxime (**PNND**) was synthesized using the procedure reported

by Muller and coworkers.[17] FTIR spectrum show the shifting to 1306 cm^{-1} of C-N band (Figure S6a). An important piece of information derived from the FTIR spectra is the appearance of a band at 1251 cm^{-1} attributed to the trans O-N=N-O isomer resulting from the self-polymerization of dinitrosobenzene (named **PNND**) at room temperature. This crucial feature is of great interest because most of the time, the oxidized version of the quinone, for example, is generally soluble and leads to a loss of capacity. The presence of a polymer in the oxidised state should make it possible to avoid such phenomena.[18] NMR spectrum of **PNND** showed the disappearance of hydroxide peak at 12.10 ppm. Moreover, all the other peaks were shifted to upfield, from 7.85-6.44 ppm to 7.23-6.65 ppm, for the presence of O-N=N-O group (Figure S5). Furthermore, TGA carried out under air atmosphere reveals that there is no trace of solvent trapped in the material structure and that PNND is thermally stable up to 200°C (Figure S6b).

3.3 Material characterization using PXRD and SEM. The crystallinity of both materials was investigated by powder X-ray diffraction (PXRD) performed with a Bruker D8 Advance diffractometer with a Cu $K\alpha_1$ and $K\alpha_2$ radiation. No diffraction peaks were detected in the powder pattern of the Li_2-BQDO (Figure S7). It is possible to conclude that this molecular material has no crystalline structure and is characterized by an amorphous ~~structure~~. XRD analysis was also performed on 1,4-phenyleneazine-N, N-dioxide (**PNND**), resulting also from the polymerization of dinitrosobenzene (**DNB**). This polymer, unlike Li_2BQD, showed a well-defined crystalline structure~~. The powder pattern collected for **PNND** was included in the Pseudo-Voigt profile function refinement~~ (Figure S8). The refined unit cell was monoclinic $P2_1/n$ with cell parameters a = 6.3913(3) Å, b = 11.29544(11) Å, c = 3.71269(5) Å, β = 92.523(4)°, and V = 267.770(14) with Bragg *R-Factor* = 0.146, R_p = 1.30, R_{wp} = 1.79 and R_{exp} = 0.72 reliability factors~~. All refined parameters, except *a*, were outside the standard deviation of those reported in Gallo and collaborators~~ (Table S1).[19] Due to the

elemental nature of the composition of **PNND** and the presence of light elements such as H ~~and Li~~, further investigation with synchrotron and/or neutron measurements are recommended for full structural refinement.

Scanning electron microscopy characterization of dioxime lithium salt and its oxidized counterpart (**PNND**) revealed a clear distinction between their shape and size. **Li_2-BQDO** appeared as irregular granules and varied in size from ~1 to 5 μm (Figure S9a). Similarly, but with a different particle shape, **PNND** showed consisted of clusters of slender parallelepipeds with a thickness around 1 μm and lengths ranging from 2 to 5 microns (Figure S9b).

3.4 Electrochemical activity of synthesized materials in half-cell configuration. As a preliminary study, the electrochemical performance of **Li_2-BQDO** were estimated using a Swagelok-type® half-cells *vs* lithium metal disk, using $LiPF_6$ in EC/DMC (50:50) electrolyte (commercially named LP30, battery grade purity). The galvanostatic profiles have been measured at C/20 (1 e^-/5 h) in 4.0-2.0 V potential window. All the electrodes were prepared using an active material/conductive carbon (KJ600) ratio of 70:30. The mixing was carried out through ball-milling for 30 minutes.

Li_2-BQDO molecule showed an average insertion potential of ca. 3.0 V (Figure 2a), higher than what reported for various organic systems, such as quinones[20] and diimides[21]. A large polarization (400 mV), possibly originated from conductivity issue, was also observed. This indicates an energy-expensive structural rearrangement during the redox process. The charge phase displayed a specific capacity of 320 mAh g^{-1}, close to the theoretical capacity of 393 mAh g^{-1}. 277 mAh g^{-1} of capacity was observed after the discharge, for 87% of reversibility during the first cycle. Despite the promising electrochemical properties shown in the first cycle, several drawbacks were observed along cycling. In the second cycle, despite no change in the oxidation capacity (331 mAh g^{-1}), the discharge capacity drops to 146 mAh g^{-1}, for a coulombic efficiency of only 44%. Moreover, a poor capacity retention was observed along

the first 10 cycles. The residual reversible capacity is only 52 mAh g^{-1}, which corresponds to a capacity retention of 21% compared to first cycle. After that, the capacity remains constant, reaching 31 mAh g^{-1} of reversible capacity after 100 cycles (Figure 2b).

This capacity fading can be explained by several phenomena. Firstly, the dissolution of the active material in the electrolyte, frequent phenomenon for small organic molecules. Another cause may be the non-optimized electrode formulation. Indeed, for the preliminary test, a simple formulation consisting in a hand-milled electrode with active material and conductive carbon was employed. The addition of binder and another mixing process can significantly improve the electrochemical properties. Lastly, the capacity fading can be addressed to side-reactions that affect the redox process, hindering the reversibility of the lithium intercalation process. About the dissolution of active material in the electrolyte, a visual analysis after 10 cycles showed no traces of active material in the separator. The dissolution of the active material in the electrolyte causes the color of the separator in contact with the electrode. As further confirmation, both benzoquinone dioxime and **PNND** were kept in a mixture of LP30 solution for one week, showing no dissolution (Figure S10). To investigate the effects of the formulation on electrochemical properties, a different formulation was prepared, with the addition of binder and changing the mixing method. In this formulation, 10w% of PVDF (binder) was added in the electrode composite, for a final ration of 60/30/10 (AM/KJ600/PVDF) and the powder was ball-milled for 30 minutes. The results obtained with this different formulation were illustrated in Figure 2c-d. Nevertheless, this formulation showed electrochemical performances almost identical to the previous one. Despite the higher specific capacity in the first charge (338 mAh g^{-1} compared to 320 mAh g^{-1} of the previous case), the discharge phase showed a large irreversibility (31%), for a reversible capacity of 233 mAh g^{-1}. In second cycle, a marked capacity drop was observed (168 mAh g^{-1} of reversible capacity), just slightly better compared to non-formulated electrode. After 100

cycles, the reversible capacity was quantified in 40 mAh g^{-1}, for an overall capacity retention of 17%, which represent only a small improvement over what was seen in the first test. In the light of the data obtained with this formulation, it is evident that the problem of capacity fading was not due to electric or ionic bad conductivity, which can usually be improved with an optimized formulation, but seems to be linked to a problem of parasitic reactions that affect the electrochemical reaction, hindering the reversibility of the lithium intercalation reaction.

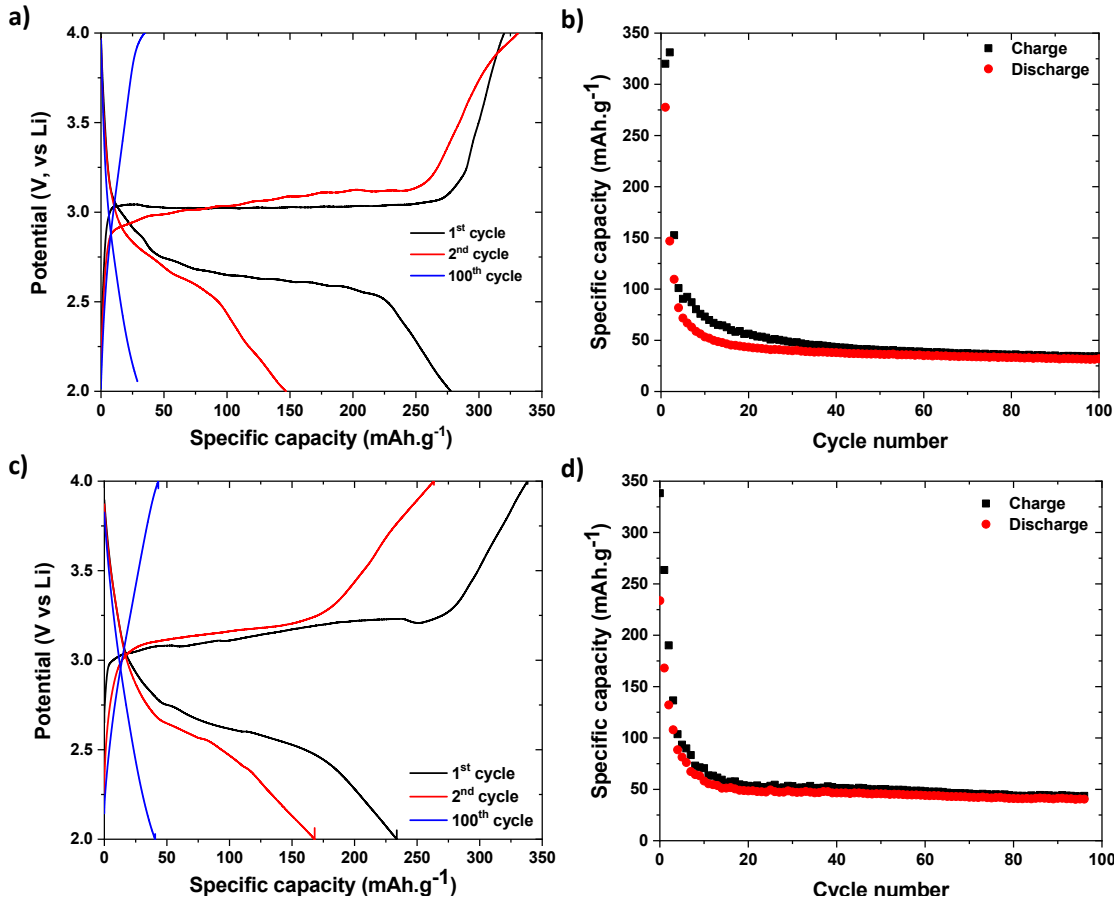

Figure 2 – (a) Galvanostatic profile of 1st, 2nd and 100th cycle and (b) corresponding capacity retention curve upon 100 cycles of Li_2BQD electrode (70:30 AM/KJ600) in half-cell vs Li, window range of 4.0-2.0 V with LP30 electrolyte. (c) Galvanostatic profile of 1st, 2nd and 100th cycle and (d) corresponding capacity retention curve upon 100 cycles of Li_2BQD electrode (60:30:10 AM/KJ600/PVDF) in half-cell vs Li, window range of 4.0-2.0 V with LP30 electrolyte.

The oxidized equivalent of benzoquinone dioxime, polymerized Dinitrosobenzene (PNND), obtained *via* chemical synthesis, was also tested in a half-cell *vs.* Li, using the same set-up described above (Figure 3). Contrary to dilithium benzoquinone dioximate, **PNND** has no Lithium ions in its structure, so the first electrochemical step was the intercalation of lithium, with relative reduction of the molecule. When the half-cell was connected to the potentiostat, a voltage of 3.9 V *vs.* Li^+/Li was measured. As reported recently, the **PNND** is above 3.0 V, the threshold below which oxidation occurs due to oxygen, confirming the air-stability of the molecule to exposure to air. The first discharge showed a specific capacity of 336 mAh g^{-1}, a value identical to that observed for the charge of the lithiated dioxime (Figure 3a). In this case, the reversible capacity was measured in 313 mAh g^{-1}, with an irreversibility of 7%, an promising result for organic materials. The average redox potential measured was 3.0 V *vs.* Li^+/Li with the same polarization, in line with what was measured in the previous cases. The second cycle showed a reduction in capacity to 268 and 293 mAh g^{-1} for discharge and charge, respectively. In the subsequent cycles, a constant loss of capacity was measured, with a consequent low retention of capacity. However, after 10 cycles, the coulombic capacity tends to become constant along cycling. After 100 charge/discharge cycles, it can be seen that the capacity value remains constant, with a specific capacity of 90 mAh g^{-1} and a coulombic efficiency of 99.5% (Figure 3b). At this stage, the origin of this reactivity is not perfectly identified, but we can assume that we have a partial dissolution of the compound which saturates the electrolyte, thus make capacitance constant.

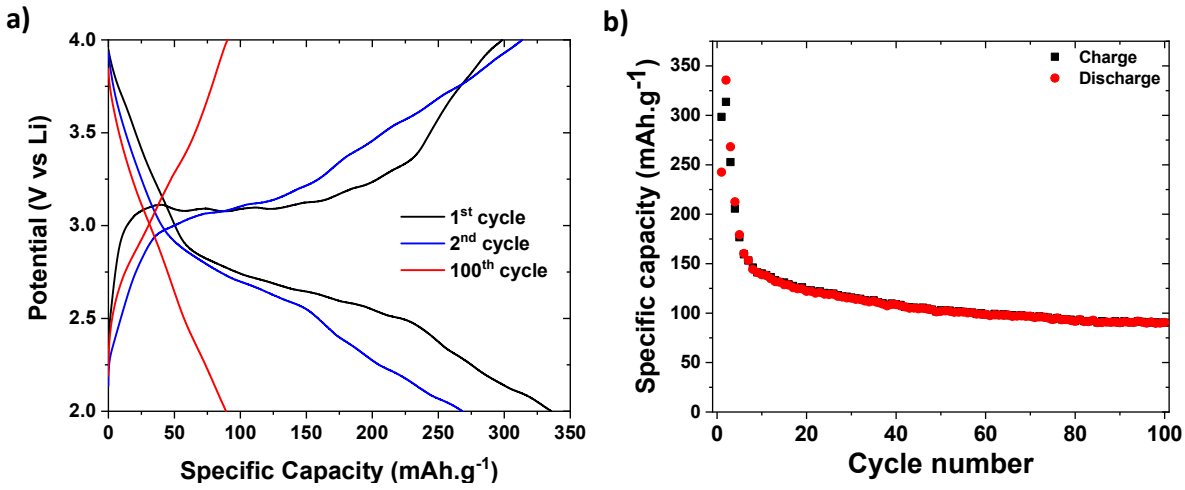

Figure 3 – (a) Galvanostatic profile of 1st, 2nd and 100th cycle and (b) corresponding capacity retention curve upon 100 cycles of PNND electrode (70:30 AM/KJ600) half-cell vs Li, window range of 4.0-2.0 V with LP30 electrolyte.

3.5 Coupled XRD and TEM investigation of the redox activity and mechanism. From the electrochemical tests performed on both the **Li_2-BQDO** and **PNND** electrodes, a marked difference emerged in terms of capacity retention along cycling. Although the redox mechanism is identical, **PNND** exhibited superior capacity stability over cycling. To investigate this important difference, *ex-situ* TEM/EELS analyses, coupled with *ex-situ* XRD diffraction, were performed on both materials, along the first complete cycle and after 20 cycles. First, a complete cycle of dilithium benzoquinone dioximate was analyzed (Figure 4a). Before cycling, **Li_2-BQDO** displays in X-ray diffraction (Figure 4b) a broad contribution with no Bragg peaks, indicating an amorphous structure. After the charging stage, with the oxidation of benzoquinone dioxime, two main Bragg peaks appeared at 2θ = 15.5° (020 reflection plane) and 2θ = 25° (011 reflection plane), indicating the appearance of crystalline phase attributed to the PNND reported structure (Figure 4b). After the discharge state (full cycle), the Bragg peaks nearly disappeared, faint peaks were visible at 2θ = 15.5° and 2θ = 25°, indicating the remaining presence of a crystalline structure. Same type of observation is obtained from XRD pattern acquired for **PNND** material (Figure 4c and d). For **PNND**,

starting material shows two diffraction peaks at 15.5° and 25.3° which vanished upon discharge and reappearing after one full cycle. It should be noted that even if an amorphous signal is observed after discharge, two new peaks are distinguished at 24° and 30.5°, which are not attributed for the moment but not present previously for **Li_2-BQDO**. After one complete cycle, in the XRD powder pattern (Figure 4b, blue line) were observed the same Bragg peaks already found in the pristine material. This result confirmed the reversibility of the redox reaction, with the full recovery of the starting crystalline structure, which is also identical to what was obtained after the oxidation of Li_2-BQDO.

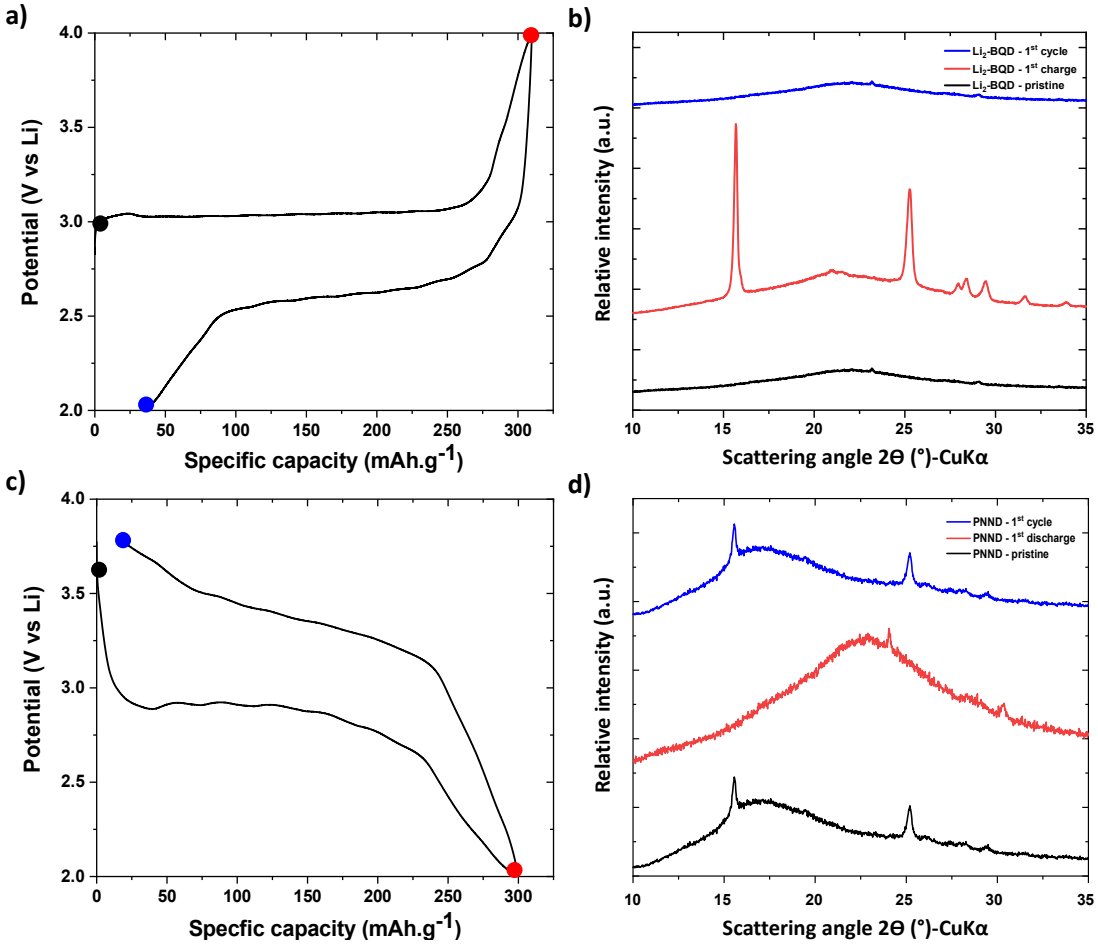

Figure 4 –Galvanostatic profile of the 1st cycle and X-ray powder patterns for (a and b) Li_2-BQDO and (c and d) PNND in pristine (black line), after half cycle (red line) and one full cycle (blue line).

The TEM investigation of **Li_2-BQDO** showed a microstructure composed of particles either round with a range diameter of 5-25 nm or needle-like with a width range of 5-25 nm and a length higher than 100 nm arranged in hollow-like agglomerates (Figure 5a). The SAED pattern (Figure 5a, inset) exhibited a diffuse ring indicating an amorphous contribution, in agreement with the XRD data. In Figure 6 is showed the chemical characterization obtained by EELS of the pristine sample about the lithium information and for the carbon and nitrogen edge. The broad and asymmetric contribution with a maximum at ~ 62 eV corresponds to the Li K-edge (Figure 6a, full black line). It will be used as reference spectrum for the lithiated phase. The white line with a sharp peak at 285 eV followed by a broad contribution at 290 eV is related to the C K-edge (Figure 6b, black full line) with respectively the π* and σ* state. A sharp peak followed by a broader contribution is also visible at 400 eV and corresponds to N K-edge (Figure 6b, black full line). The presence of the nitrogen contribution confirmed the presence of active material in the investigated area. The microstructure of the electrochemically oxidized Li_2-BQDO exhibits marked differences (Figure 5b) with large particles of irregular shape and a size ranging from 500 nm and up to 2.5 μm. They form relatively large and homogeneous masses as highlighted by white area according the (00-1) in the dark field image (red circle in Figure S10b and arrow in Figure S10c, ESI). By investigating them closely, some small, rounded grains (~ 5-25 nm) can be distinguished and seem to be "glued" to the big particles. These observations are consistent with a growth process and most probably here with a progressive polymerization of small organic grains as proposed by Wang *et al.*[13] The SAED pattern obtained on the large particles present a dots pattern (see inset in Figure 5b), which is characteristic of mono-crystalline sample and the indexation of the direction can be in accord with (00l) interplanar distance from **PNND** (Figure S11b).[19] The chemical characterizations obtained by EELS showed the absence of contribution in the Li K-edge (Figure 6a, black dot line) and the presence of white lines in the

C K-edge and N K-edge (Figure 6b, black dot line) confirming that the crystalline area was the active material and the complete lithium de-insertion after the charge process. The microstructure after discharged sample showed relatively large, separated and porous area. The diffraction pattern collected in this area exhibited defined rings, indicating a polycrystalline character. The dark field image obtained on the discharged sample highlighted the presence of small white areas (red arrows in Figure S12f), which diffract according to the red circles (Figure S12e) and were distributed randomly. The inter-reticular distances determined from the diffraction pattern (see Figure S9c) are d_1 = 4.2 Å, d_2 = 3.0 Å et d_3 = 2.52 Å. The chemical characterizations of discharged sample obtained by EELS showed the presence of a contribution in the Li K-edge (Figure 6a, black dot line) similar to the pristine sample. Moreover, the presence of white lines in the C K-edge and N K-edge (Figure 6b, black dot line) confirmed the lithium re-intercalation in the active material during the discharged process. The analysis of small crystalline area showed a fast amorphization under the electron beam, as well as the characterization *via* EELS was performed in an average way.

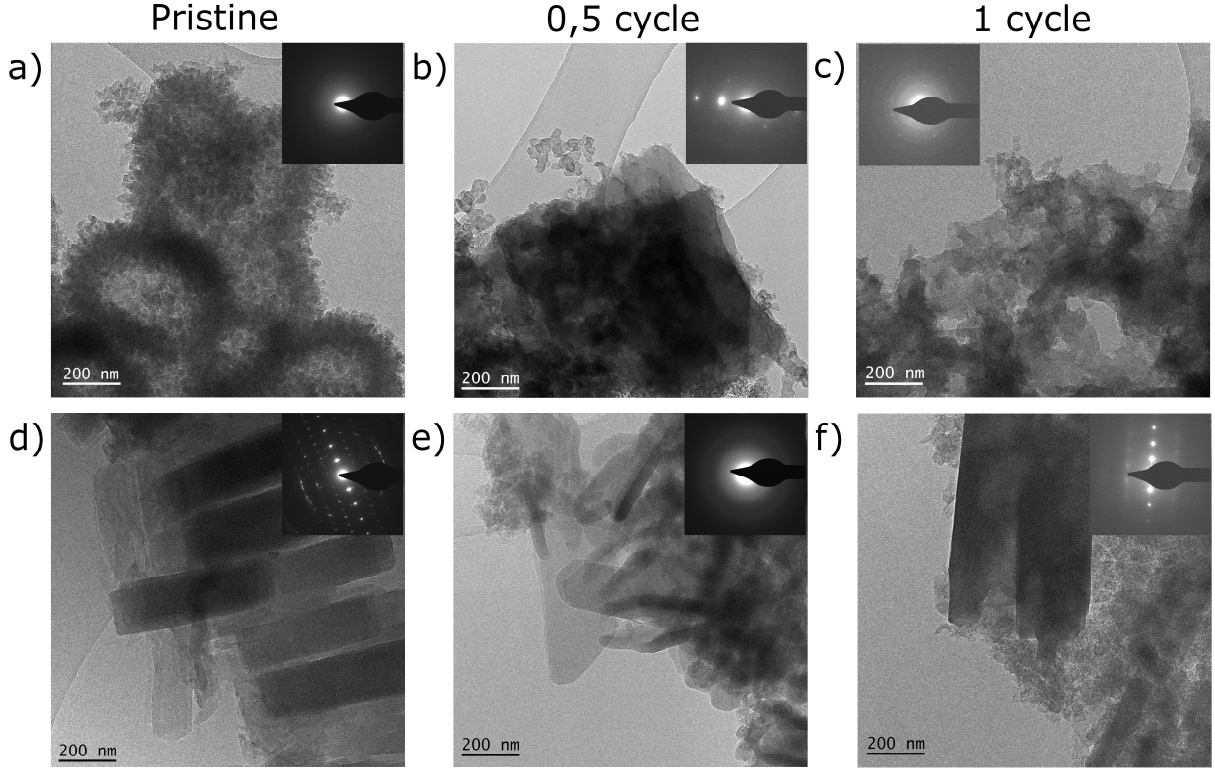

Figure 5 - TEM bright field images of Li_2BQD (a) pristine, after (b) half cycle and (c) one full cycle. TEM bright field images of PNND d) pristine, after e) half cycle and f) one full cycle. The associated diffraction patterns are in inset (and in Figure S7 ESI).

The TEM analysis of the first complete cycle was also performed starting from PNND (Figure 5d-f). The images showed significant differences compared to the PNND obtained *via* electro-oxidation from **Li_2-BQDO**. The microstructure was formed of needle-like particles, which were arranged to form rectangular parallelepipeds, with lateral dimensions between of 150-200 nm and lengths ranging up to 1-2 microns. The SAED patterns recorded on **PNND** parallelepiped particles showed similar pattern (Figure 5d, inset), with arranged dots corresponding to a monocrystalline phase and their indexation in agreement with the **PNND** in the zone axis [001] (Figure S9d), indicating a preferential orientation growth. The EELS reference spectra (Figure 6a and 8b, dark blue full line) showed the absence of lithium, consistent with the oxidized form that does not have lithium ions in the structure, and the presence of carbon and nitrogen confirming the presence of the active material. However, the π^* state at 285 eV in the C-K edge is less intense compared to what observed with Li_2-BQDO. After discharging the sample, the complete amorphization of the crystalline structure was confirmed by X-ray diffraction, where the disappearance of the Bragg peaks was observed in the powder pattern (Figure 4d, red line). The microstructure at the discharged state was evolved. The visible parallelepiped particles showed a smoother edge, but also other particles with 30-65 nm thick wall were observed in the image. The latter can be connected or not by a thinner area in the middle, as little like trivia monacha (Figure 5e). The associated diffraction pattern is composed of diffuse rings indicating an amorphous structure which is coherent with the X-ray diagram. The EELS investigation on the Li-K edge (Figure 6a, dark blue dot line) highlighted the presence of lithium, for which the shape and position of the main peaks fit

with what observed for **Li_2-BQDO**. The presence of active material was confirmed by the presence of carbon and nitrogen peaks (Figure 6b, dark blue dot line).

The microstructure did not change after the charge phase. The shape and size of active material particles is similar to the discharged state, with particles with 30-65 nm thick wall connected or not by a thinner area in the middle, as can be seen in Figure 5f. The associated diffraction pattern (inset Figure 5f and Figure S11f) is composed of dots arranged in a motif indicating a crystalline sample. This result is coherent with the XRD measurement, but the signal is less intense compared to the pristine sample. The indexation of diffraction peaks is compatible with **PNND** crystalline structure, but with the modification in the intensity distribution can indicate a slight change in the orientation of the crystal structure particles. Finally, the EELS analysis on the Li-K edge (Figure S13a, dark blue dash-dot line) showed the absence of lithium, confirming the reversibility of the lithium de-/insertion redox process. As in the previous case, the presence of the active material in the investigated zone was confirmed by C-/N-K edges (Figure S14b, dark blue dash-dot line).

The results observed from the coupled TEM / XRD analysis over a full cycle, starting from both Li_2-BQDO and **PNND**, may explain the differences, in terms of electrochemical properties, between the two materials. Although the crystal structure remained unchanged for all states involving dinitrosobenzene, as confirmed by TEM diffraction and *ex-situ* XRD analysis, the microstructure was strongly different depending on the type of process (chemical or electrochemical) used to obtain the polymeric equivalent (**PNND**). These differences in the microstructures of **PNND**, both in the uncontaminated monomeric form and in the **PNND** polymer form, can profoundly affect the lithium deactivation / insertion process during the cycle. The radiation obtained through direct chemical synthesis is more orderly and oriented than PNND obtained by electrochemistry, resulting in an improvement in the diffusion and insertion of lithium ions in the active material, with a consequent improvement in

electrochemical performance, especially for regarding retention of capacity. Such finding is interesting and should be investigate in more details in the future to maximize capacity.

In addition to studying the first complete redox cycle, TEM analysis was used to investigate the differences between the two electrodes after 20 charge and discharge cycles, in order to understand the observed differences in term of capacity retention (Figure 6). As observed in the capacity vs. cycles profiles, most of the loss of capacity occurs, in both cases, in the first 20 cycles, then it remains constant. The TEM images (Figure 6a) showed, in the case of the benzoquinone dioxime electrode after 20 complete cycles, a microstructure composed of irregularly shaped particles, characterized by marked porosity, since the color scale in the particles is inhomogeneous (one of these areas is surrounded by the dashed line in Figure 9a). Furthermore, the presence of thin sheets was also observed, as highlighted by the white arrow in Figure 9a. The associated diffraction pattern in negative mode (Figure 6b) is composed of a defined weak ring indicating the polycrystalline nature of this microstructure (irregular particles + thin sheets). The inter-lattice distances d_1 and d_2 are respectively approximately 4.4 Å and 2.6 Å, but the information was insufficient to obtain the adequate indexation.

About the **PNND**-based electrode after 20 cycles (Figure 6c), it was also composed of irregular shape particles which also was characterized by porous structure. In this case, the presence of the thin sheets and their associated diffraction pattern was not observed. The electron diffraction showed diffuse rings indicating the amorphous nature of the material. The EELS analysis of Li_2-BQDO after 20 cycles shows the presence of phosphorus, lithium, carbon, oxygen and fluorine relative to the areas where the polycrystalline thin sheets are present (Figure S14). These elements, deriving from the electrolytic salt, indicate the presence of derivatives from the degradation of electrolyte. These polycrystalline structures and their

relative chemical composition were not detected in the dinitrosobenzene electrode indicating in the latter case the degradation of the electrolyte is less marked.

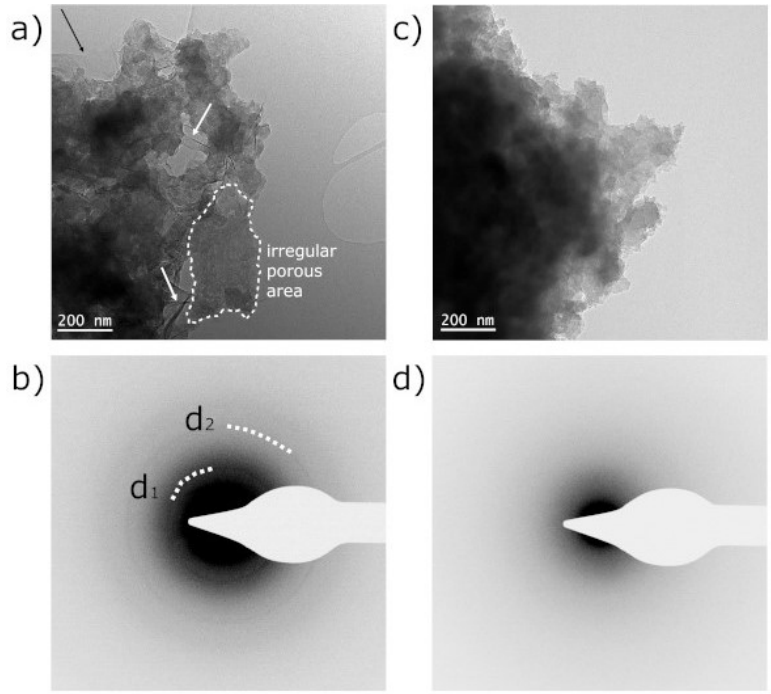

Figure 6 - a) TEM bright field images and b) associated diffraction patterns of Li_2-BQDO after 20 cycles; c) TEM bright field images and d) associated diffraction patterns of PNND after 20 cycles.

The phenomenon of electrolyte degradation can be used as an explanation for the greater loss of capacitance on the part of the Li_2-BQDO compared to the PNND. As further perspective, a more in-depth analysis on the causes of this phenomenon will help to obtain a more comprehensive understanding of the electrochemical properties of these materials, in order to understand the possible chemical-physical modifications necessary to improve their performance.

4. Conclusions

In the present work, a global approach in the study of benzoquinone dioxime derivatives as a positive material for lithium-ion batteries was reported. By following a DFT molecular

modelling performed prior to any experiment and aimed at providing a first glimpse of the redox mechanism characterizing DNB and Li_2-BQDO systems, the synthesis and characterization of the dioxime derivatives were performed, both in the lithiated form and in the delithiated polymerized (PNND) form. The materials were characterized through SEM and XRD analyzes and showed an average redox potential of 3.0 V *vs.* Li^+/Li, with a promising specific capacity in the first cycle, measured in 277 and 313 mAh g^{-1} for Li_2-BQDO and PNND, respectively but exhibited low capacity retention low over long cycling, with only 11% and 23% retention after 100 cycles. Thanks to a pool of techniques the redox mechanism of insertion /desinsertion of lithium ions in the active material was investigated. It was found that the difference of microstructure is the basis of the different electrochemical performances observed in galvanostatic tests which is better in the case of the chemically oxidized version. The marked formation of salts originating from the degradation of the electrolyte was observed in the case of the Li_2-BQDO electrode, which allows to point to this phenomenon the greater loss of capacity observed. This study allowed to understand in detail the redox mechanism of benzoquinone dioxime, validating the proposed model both through simulations and experimental tests. The exceptional electrochemical properties shown, such as the insertion potential of 3.0 V *vs.* Li^+/Li and the specific capacity greater than 300 mAh g^{-1} observed in the first cycle open the way for future studies on derivatives of benzoquinone dioxime as eco-sustainable positive materials for lithium batteries.

Conflicts of interest

There is no conflict of interest to declare.

Acknowledgements

Financial support from the ANRT is gratefully acknowledged for partially supporting the funding of this research work between LRCS and EDF (Convention CIFRE N° 2019/0926).

The authors also deeply thank D. Cailleux and M. Courty respectively for NMR and TGA analysis.

References

(1) Poizot, P.; Dolhem, F. Clean Energy New Deal for a Sustainable World: From Non-CO2 Generating Energy Sources to Greener Electrochemical Storage Devices. *Energy and Environmental Science* 2011, *4,* 6, 2003–2019.
(2) Armand, M.; Axmann, P.; Bresser, D.; Copley, M.; Edström, K.; Ekberg, C.; Guyomard, D.; Lestriez, B.; Novák, P.; Petranikova, M.; Porcher, W.; Trabesinger, S.; Wohlfahrt-Mehrens, M.; Zhang, H. Lithium-Ion Batteries – Current State of the Art and Anticipated Developments. *Journal of Power Sources* 2020, 479, 228708.
(3) Goodenough, J. B.; Park, K. S. The Li-Ion Rechargeable Battery: A Perspective. *Journal of the American Chemical Society* 2013, 135, 4, 1167–1176.
(4) Poizot, P.; Gaubicher, J.; Renault, S.; Dubois, L.; Liang, Y.; Yao, Y. Opportunities and Challenges for Organic Electrodes in Electrochemical Energy Storage. *Chemical Reviews* 2020, 120, 14, 6490–6557.
(5) Armand, M.; Tarascon, J.-M. Building Better Batteries. Nature 2008, 451, 1, 652–657.
(6) Larcher, D.; Tarascon, J. M. Towards Greener and More Sustainable Batteries for Electrical Energy Storage. Nature Chemistry 2015, 7, 1, 19–29.
(7) Lakraychi, A. E.; Vlad, A. Organic Batteries: The Route Toward Sustainable Electrical Energy Storage Technologies. *Chimie Nouvelle* 2018, 127, 1–9.
(8) Fédèle, L.; Sauvage, F.; Lepoivre, F.; Gottis, S.; Davoisne, C.; Courty, M.; Tarascon, J. M.; Becuwe, M. Mesoscale Texturation of Organic-Based Negative Electrode Material through in Situ Proton Reduction of Conjugated Carboxylic Acid. *Chemistry of Materials* 2019, 31*,* 16, 6224–6230.
(9) Lakraychi, A. E.; Dolhem, F.; Vlad, A.; Becuwe, M. Organic Negative Electrode Materials for Metal-Ion and Molecular-Ion Batteries: Progress and Challenges from a Molecular Engineering Perspective. *Advanced Energy Materials* 2021, 11 32, 1–28.
(10) Min, D. J.; Lee, K.; Park, S. Y.; Kwon, J. E. Mellitic Triimides Showing Three One-Electron Redox Reactions with Increased Redox Potential as New Electrode Materials for Li-Ion Batteries. *ChemSusChem* 2020, 13*,* 9, 2303–2311.
(11) Park, H.; Shuku, Y.; Lee, J.; Lee, K.; Joo Min, D.; An, B.-K.; Awaga, K.; Young Park, S.; Eon Kwon, J. Isomeric Triptycene Triquinones as Universal Cathode Materials for High Energy Alkali Metal Batteries. *Batteries & Supercaps* 2023, 6, 3, e202200497.
(12) Chen, H.; Armand, M.; Demailly, G.; Dolhem, F.; Poizot, P.; Tarascon, J. M. From Biomass to a Renewable LiXC6O6 Organic Electrode for Sustainable Li-Ion Batteries. *ChemSusChem* 2008, 1, 4, 348–355.
(13) Wang, J.; Apostol, P.; Rambabu, D.; Guo, X.; Liu, X.; Robeyns, K.; Du, M.; Zhang, Y.; Pal, S.; Markowski, R.; Lucaccioni, F.; Lakraychi, A. E.; Morari, C.; Gohy, J.-F.; Gupta, D.; Vlad, A. Revealing the Reversible Solid-State Electrochemistry of Lithium-Containing Conjugated Oximates for Organic Batteries. *Science Advances* 2023, 9, 17, eadg6079.
(14) Dupont, L.; Laffont, L.; Bodenez, V.; Tarascon, J.-M. Recent Developments in Transmission Electron Microscopy Techniques to the Characterization of Cycled Li-Ion Electrode Materials. *ECS Meeting Abstracts* 2006, MA2006-02, 5, 349–349.
(15) R. Rathore; J. S. Kim; J. K. Kochi. Catalytic Autoxidation of Benzoquinone Dioximes with Nitrogen Oxides: Steric Effects on the Preparation of Monomeric

Dinitrosobenzenes. *Journal of Chemical Information and Modeling* 1994, 1, 9, 2675–2684.
(16) Lakraychi, A. E.; Dolhem, F.; Djedaïni-Pilard, F.; Thiam, A.; Frayret, C.; Becuwe, M. Decreasing Redox Voltage of Terephthalate-Based Electrode Material for Li-Ion Battery Using Substituent Effect. *Journal of Power Sources* 2017, 359, 198–204.
(17) Burkhard Miller; Calaminus;, B.; Beiersdorf;, W.-D.; Gruber;, W.; Hoffman, H.-J.; RainerWefringhaus; Kuhm, P.; Block, C.; Hibner, N. P-DINITROSOBENZENE - United States Patent. **1999**, US5976402A.
(18) Mutlu, H.; Kusefoglu, S. H. Synthesis and Characterization of Polymers from Soybean Oil and P-Dinitrosobenzene. *Journal of Applied Polymer Science* 2009, 113, 1925–1934.
(19) Gallo, G.; Mihanović, A.; Rončević, I.; Dinnebier, R.; Vančik, H. Crystal Structure and ON-OFF Polymerization Mechanism of Poly(1,4-Phenyleneazine-N,N-Dioxide), a Possible Wide Bandgap Semiconductor. *Polymer* 2020, 214, 123235.
(20) Han, C.; Li, H.; Shi, R.; Zhang, T.; Tong, J.; Li, J.; Li, B. Organic Quinones towards Advanced Electrochemical Energy Storage: Recent Advances and Challenges. *Journal of Materials Chemistry A*, 2019, 7, 23378-23415
(21) Vadehra, G. S.; Maloney, R. P.; Garcia-Garibay, M. A.; Dunn, B. Naphthalene Diimide Based Materials with Adjustable Redox Potentials: Evaluation for Organic Lithium-Ion Batteries. *Chemistry of Materials* 2014, 26, 24, 7151–7157.

Graphic for manuscript